Journal of Organometallic Chemistry 694 (2009) 988–1000

Contents lists available at ScienceDirect

Journal of Organometallic Chemistry

journal homepage: www.elsevier.com/locate/jorganchem

Tuning photophysical properties with ancillary ligands in Ru(II) mono-diimine complexes

Ayesha Sharmin [a], Reuben C. Darlington [a], Kenneth I. Hardcastle [b], Mauro Ravera [c], Edward Rosenberg [a,*], J.B. Alexander Ross [a,*]

[a] Department of Chemistry and Bio-Chemistry, University of Montana, Missoula, MT 59812, USA
[b] Department of Chemistry, Emory University, Atlanta, GA 30322, USA
[c] Dipartimento di Scienze dell_Ambiente e della Vita, Universita' del Piemonte Orientale "Amedeo Avogadro", Spalto Marengo 33, 15100 Alessandria, Italy

ARTICLE INFO

Article history:
Received 16 October 2008
Received in revised form 19 November 2008
Accepted 20 November 2008
Available online 30 November 2008

Keywords:
Ruthenium complexes
Metal-to-ligand charge-transfer
Photophysical properties
Electrochemistry
Phosphine ligands

ABSTRACT

The series of complexes $[XRu(CO)(L–L)(L')_2][PF_6]$ (X = H, TFA, Cl; L–L = 2,2′-bipyridyl, 1,10-phenanthroline, 5-amino-1,10-phenanthroline and 4,4′-dicarboxylic-2,2′-bipyridyl; $L'_2 = 2PPh_3$, $Ph_2PC_2H_4PPh_2$, $Ph_2PCH{=}CHPPh_2$) have been synthesized from the starting complex $K[Ru(CO)_3(TFA)_3]$ ($TFA = CF_3CO_2$) by first reacting with the phosphine ligand, followed by reaction with the L–L and anion exchange with $NaPF_6$. In the case of L–L = phenanthroline and $L'_2 = 2PPh_3$, the neutral complex $Ru(Ph_3P)(CO)$(1,10-phenanthroline)$(TFA)_2$ is also obtained and its solid state structure is reported. Solid state structures are also reported for the cationic complexes where L–L = phenanthroline, $L_2 = 2PPh_3$ and X = Cl and for L–L = 2,2′-bipyridyl, $L_2 = 2PPh_3$ and X = H. All the complexes were characterized in solution by a combination of ^1H and ^{31}P NMR, IR, mass spectrometry and elemental analyses. The purpose of the project was to synthesize a series of complexes that exhibit a range of excited-state lifetimes and that have large Stokes shifts, high quantum yields and high intrinsic polarizations associated with their metal-to-ligand charge-transfer (MLCT) emissions. To a large degree these goals have been realized in that excited-state lifetimes in the range of 100 ns to over 1 μs are observed. The lifetimes are sensitive to both solvent and the presence of oxygen. The measured quantum yields and intrinsic anisotropies are higher than for previously reported Ru(II) complexes. Interestingly, the neutral complex with one phosphine ligand shows no MLCT emission. Under the conditions of synthesis some of the initially formed complexes with X = TFA are converted to the corresponding hydrides or in the presence of chlorinated solvents to the corresponding chlorides, testifying to the lability of the TFA Ligand. The compounds show multiple reduction potentials which are chemically and electrochemically reversible in a few cases as examined by cyclic voltammetry. The relationships between the observed photophysical properties of the complexes and the nature of the ligands on the Ru(II) is discussed.

© 2008 Elsevier B.V. All rights reserved.

1. Introduction

Transition metal luminescent complexes containing one or more diimine ligands typically have excited-state lifetimes ranging from about 100 ns to 10 μs. Because the lifetimes of these luminophores are long compared to fluorescent dyes that are used as biological probes, time-gated detection can be used to suppress interfering auto-fluorescence from the biological sample. In addition, highly polarized emission from some of these complexes has stimulated interest in using them as biophysical probes for studying the dynamics of macromolecular assemblies and interactions on membranes [1–4]. The luminescent behavior of these complexes arises from the MLCT (metal-to-ligand charge-transfer) band. Because the emission of metal–ligand complexes (MLCs) is dominated by the MLCT transition, the MLCs behave like a single chromophoric unit, and they have high chemical and photochemical stabilities under physiological conditions. As a result of these favorable properties, MLCs are finding new applications in biophysical chemistry, clinical chemistry and DNA diagnostics [5,6].

Because the energy gap law determines the luminescent properties of these complexes, several criteria must be satisfied to observe luminescence from their MLCT state [7–10]. The ligand field must be strong enough to raise the d–d state above the MLCT state [11]. This is the reason why $[Fe(L–L)_3]^{2+}$ are not luminescent (non-radiative decay), but $[Ru(L–L)_3]^{2+}$ show radiative decay and hence useful luminescence (L–L = 2,2 bipyridyl, 1,10-phenanthroline and their derivatives). However, the energy of the excited-state

* Corresponding authors. Tel: +1 406 243 2592; fax: +1 406 243 6026 (E. Rosenberg); tel./fax: +1 406 243 4227 (J.B. Alexander Ross).
E-mail addresses: edward.rosenberg@mso.umt.edu (E. Rosenberg), sandy.ross@umontana.edu (J.B. Alexander Ross).

0022-328X/$ - see front matter © 2008 Elsevier B.V. All rights reserved.
doi:10.1016/j.jorganchem.2008.11.048

is closer to the ground state for the Os–MLCs. Consequently, they typically show weak luminescence; the smaller energy gap facilitates non-radiative decay [5]. The luminescence of these complexes is phosphorescence from the triplet state. Because of the strong spin–orbit coupling, the intersystem crossing from the initially excited singlet state is very efficient, and the triplet excited-state yield is close to unity. In addition, the degree of singlet–triplet mixing directly affects the radiative vs. non-radiative decay rates, and thus affects the lifetime of the resulting triplet excited-state. In particular, increased singlet–triplet mixing results in shorter triplet excited-state lifetimes.

When excited with polarized light, the emission from asymmetric MLCT complexes is also polarized, which makes these complexes useful for studying dynamics; in general, complexes with non-identical diimine ligands show higher fundamental anisotropies than the more symmetrical complexes. The first such complex reported was $[Ru(bpy)_2(dcbpy)]^{2+}$ (dcbpy = 4,4′-dicarboxy-2,2′-bipyridyl). This dicarboxy derivative showed higher fundamental anisotropies than $[Ru(bpy)_3]^{2+}$. Introducing electron withdrawing groups on the diimine ligand resulted in red-shifted emission and an increase in emission anisotropy, which suggests that one ligand is accepting an electron preferentially in the MLCT transition [1,12–14]. The possibility of improving the fundamental anisotropy with a single chromophoric ligand in metal–ligand complexes is based on results for Re(I) complexes (e.g. [Re(4,7-dimethylphen)$(CO)_3$(4-carboxy-Py)(PF_6)]) [4,15].

A limitation of most metal–ligand complexes is low quantum yield. However, the electronic effect of ligands on the energy gap can be utilized to increase quantum efficiency. Previous studies [16] have shown that replacing diimines with chelating phosphine ligands results in increased quantum yields of $[Os(phen)(dppene)]^{2+}$ and $[Os(phen)_2(dppene)]^{2+}$ (dppene = diphenylphosphinoethylene) compared to $[Os(phen)_3]^{2+}$ ($Q = 0.518$, 0.138 and 0.016 respectively). Therefore, careful selection of metal and ligands can generate MLCs with spectroscopic and physical properties useful for the study of specific biological systems [5,9,17–20]. For example, we recently reported the synthesis, electrochemical and electrogenerated chemiluminescence studies of $[Ru(bpy)_2\{2\text{-}(4\text{-methylpyridine-2-yl})benzo[d]\text{-}X\text{-}azole\}(PF_6)_2]$ [21]. This study focused on the development of novel electrogenerated chemiluminescence devices suitable for the detection of different biological analytes of clinical and environmental interest. Also, Lakowicz and coworkers have reported the use of the long-lifetime probe [Re(4,7-dimethyl-phen)$(CO)_3$(4-carboxy-Py)(PF_6)] to study overall rotational motion in lipid vesicles and microsecond dynamics of cell membranes [2–4]. The limitation of this type of complex is that the ligation around the metal is not amenable to further modification because the carbonyls are difficult to substitute, making it difficult to further alter the excited-state lifetime.

To develop better MLC probes for application to specific biological systems, a deeper understanding of the probe's photophysical properties is required. Recently, we reported photophysical and computational studies of $[Re(CO)_3\{2\text{-}(4\text{-methyl pyridine-2-yl})benzo[d]\text{-}X\text{-}azol\}L]$ and $[Re(CO)_3\{2\text{-}(4\text{-methylpyridine-2-yl})benzo[d]\text{-}X\text{-}azol\text{-}2\text{-}yl\}(4\text{-methylquinolin})L]^+$. The purpose of these studies was to investigate the effect of the organic ligand on the optical properties and electronic structure of the reported complexes [22]. The results showed that the photophysical properties depended on the nature of X (N > S > O) and L (py and Cl). The pyridinyl nitrogen is a better electron donor for the Ru(II), and this donor results in a higher quantum yield and longer excited-state lifetime relative to the S and O containing heterocycles.

Ideally, one would like to develop a series of complexes where the MLCT band is red-shifted and well-separated from the intraligand transitions and where the intensity of the MLCT transition is stronger than observed for previously reported Ru(II) diimine complexes. It would be desirable to have the ability to tune the lifetime of the excited-state so that one could tailor a particular probe to a particular dynamical process in a bio-macromolecule. It would also be desirable to have complexes that contain only one chelating heterocycle, because this would decrease the molecular symmetry, which would have the effect of increasing the anisotropy of the luminescence. Combining all of these desired features into the synthesis of a luminescent probe is a challenging task. However, by making use of the easily-substituted ruthenium complex $K[Ru(CO)_3(TFA)_3]$ [23] and the well-known fact that the incorporation of π-acid ligands [5,16,24] into complexes containing chelating nitrogen heterocycles has the effect of prolonging the excited-state lifetime [16], we have developed synthetic pathways to complexes having most, if not all, of the desired photophysical properties. In this study, we report the synthesis of a series of complexes $[XRu(CO)(L\text{–}L)(L')_2][PF_6]$ (X = H, TFA, Cl; L–L = 2,2′-bipyridyl, 1,10-phenanthroline, 5-amino-1,10-phenanthroline and 4,4′-dicarboxylic-2,2′-bipyridyl; $(L')_2 = 2PPh_3$, $Ph_2PC_2H_4PPh_2$, $Ph_2PC_2H_2PPh_2$).

2. Experimental

2.1. General methods and materials

Reactions were carried out under a nitrogen atmosphere, but purification was carried out in air using preparative thin layer chromatography (10 × 20 cm plates coated with 1 mm silica gel PF 60254-EM Science). Activated neutral alumina (size) was also used to purify compounds by column chromatography. Solvents were reagent grade. Tetrahydrofuran was distilled from benzophenone ketyl and methylene chloride and acetonitrile were distilled from calcium hydride. Ruthenium carbonyl was purchased from Strem Chemicals. 2,2-bipyridyl, 1,10-phenantroline, 4,4′-dicarboxy-2,2-bipyridyl and 5-amino-1,10-phenanthroline (Aldrich) were used as received. ^1H NMR spectra were obtained on a Varian 400 MHz Unity Plus or a Varian NMR Systems 500 MHz spectrometer. Infrared spectra were obtained on a Thermo-Nicolet 633 FT-IR spectrometer. Elemental analyses were performed by Schwarzkopf Microanalytical Labs, Woodside, NY. ESI-MS spectra ware obtained on a Watts/Micromass LCT using 80% MeCN as carrier solvent. Some of the spectra showed the presence of Na^+ associated with the molecular ion due to the extensive use of salt solutions with this instrument which has contaminated the analyzer.

2.2. Crystal structure analysis

Suitable crystals of **5**, **6** and **10** were coated with Paratone N oil, suspended in a small fiber loop and placed in a cooled nitrogen gas stream at 173 K on a Bruker D8 SMART APEX CCD sealed tube diffractometer with graphite-monochromated Mo Kα (0.71073 Å) radiation. Data were measured using a series of combinations of phi and omega scans with 10 s frame exposures and 0.30 frame widths. Data collection, indexing and initial cell refinements were all carried out using SMART [25] software. Frame integration and final cell refinements were done using SAINT [26] software. The final cell parameters were determined from least-squares refinement on 2481 and 5705 reflections, respectively. The SADABS [27] program was used to carry out absorption corrections. The structure was solved using the Patterson method and difference Fourier techniques (SHELXTL, V6.12) [28]. Hydrogen atoms were placed in their expected chemical positions using the HFIX command and were included in the final cycles of least-squares with isotropic Uij's related to the atom's ridden upon. All non-hydrogen atoms were refined anisotropically. Scattering factors and anomalous dispersion corrections are taken from the *International Tables for X-ray Crystallography* [29]. Structure solution, refinement, six graphics and

Table 1
IR, NMR and ESI-MS data.

Compound	IR (ν_{CO}, cm^{-1})[a]	^1H NMR (δ, ppm)[b]	^{31}PNMR (δ, ppm)[b]	ESI-MS[c] (m/z)
2	2061vs, 2001vs, 1692vs	7.8–7.2 (30H)	29.52(s, 2P)	794 [M−TFA]
3	2066vs, 2004vs, 1691vs	7.8–7.0 (20H), 3.6–3.4 (2H), 2.01 (2H)	45.8 (s, 1P), 44.07(s, 1P)	–
4	2077vs, 2006vs, 1692vs	7.8–6.9 (22H)	53.99(s, 1P), 53.47(s, 1P)	–
5	1993vs, 1688s	8.9–8.2 (6H), 7.9–6.8 (32H)	26.6(s, 2P), −155(1P)	869 [M−PF_6]
6	1982s, 1703vs	9.4–8.2 (6H), 7.8–6.9 (17H)	28.3(s, 1P), −155(1P)	685 [M−TFA]
7	1992vs, 1680s	9.1–8.4 (6H), 7.8–6.9 (32H),	28.98 (s, 2P), −155 (1P)	923 [M−PF_6]
8	1992s, 1727s, 1680m	–	–	–
9	1944s, 1730s	11.7 (2H), 9.1–8.5 (4H), 6.9–8.1 (32H), −11.09 (1H)	50.9 (2P), −155 (1P)	943[M−PF_6+2Na^+]
10	1942s	9.0–8.2 (6H), 7.8–6.9 (32H), −11.07 (1H)	50.45 (2P), −155 (1P)	811 [M−PF_6]
11	1988vs, 1692m	8.6–7.9 (4H), 7.7–6.6 (23H), 3.6–3.3 (2H), 2.04 (2H)	45.24 (2P), −155 (1P)	967 [M+H^+]
12	1987vs, 1704m	9.4–8.2 (6H), 8.0–6.7 (22H), 3.5–3.3 (2H), 2.04 (2H)	53.96 (2P), −155 (1P)	941 [M^+]
13	1992vs, 1691m	8.8–8.2 (4H), 7.9–7.2 (23H), 7.0–6.8 (3H)	49.93 (2P), −155 (1P)	965 [M+H^+]
14	1988vs, 1706m	8.9–8.1 (6H), 7.8–6.8 (24H)	53.93 (2P), −155 (1P)	939 [M^+]
15	1990vs, 1685m	8.75–8.05 (5H), 7.8–7.0 (22H), 4.9–4.6 (2H)	53.9 (2P), −155 (1P)	835 [M−PF_6]
16	1977s	8.3–7.9 (5H), 7.8–6.8 (22H), 4.0 (2H), −7.4 (1H)	74.8 (2P), −155 (1P)	723 [M−PF_6]

[a] Data were collected in KBr.
[b] Data were collected in Acetone d^6.
[c] Data were collected in 80% acetonitrile.

generation of publication materials were performed by using SHELXTL, V6.12 software. Additional details of data collection and structure refinement are given in Table 2.

2.3. Electrochemistry

A PAR 263A electrochemical analyzer (EG&G Princeton Applied Research, Oak Ridge, TN, USA) interfaced to a personal computer running PAR M270 electrochemical software was used for the electrochemical measurements. A standard three-electrode cell was designed to allow the tip of the reference electrode (saturated calomel electrode, SCE) to closely approach the working (a glassy carbon disk, diameter 0.1 cm, sealed in epoxy resin), and the auxiliary (a Pt wire) electrodes. All measurements were carried out under nitrogen in CH_2Cl_2 solutions containing 0.1 M $[NBu_4]PF_6$ as supporting electrolyte and the metal complexes at 1.0×10^{-3} M. All potentials are reported vs. the ferrocene/ferrocinium redox couple, added as an internal standard ($E^{o\prime}$ (Fc/Fc^+) = +0.41 V vs. SCE [i]). Positive-feedback IR compensation was applied routinely [30].

2.4. Luminescence spectroscopy

Steady state UV–Vis absorption spectra and emission spectra were recorded on a Molecular Devices Spectra Max M2. The quantum yields (Φ) for the luminescent complexes in the presence of oxygen were calculated using Eq. (1), relative to a Rhodamine B standard (Φ = 0.7 3, in ethanol), where abs is the absorbance (<0.05) at the excitation wavelength (420 nm), and area is the integrated emission spectrum corrected for the wavelength-dependent quantum efficiency of the instrument [31].

$$\Phi = \frac{\text{abs Rhodamine}}{\text{area Rhodamine}} \times \frac{\text{area Ru}}{\text{abs Ru}} \times 0.73 \quad (1)$$

Time-resolved luminescence decay and anisotropy decay measurements were performed by time-correlated single-photon counting (TCSPC), using the Quantum Northwest FLASC 1000 sample chamber (Spokane, WA). In the FLASC 1000, the vertical (V or 0° to vertically polarized excitation) and horizontal (H or 90°) emission components are separated on one side of the sample cuvette, orthogonal to the excitation path, by a beam-splitting Glan-Thompson polarizer (Karl Lambrecht, Chicago, IL). This allows *simultaneous* detection of the V and H anisotropy decay components by separate detectors, which assures data collection under identical excitation conditions. A variable-angle polarizer, in the emission path on the opposite side of the sample cuvette, was set at the magic angle (54.7° to vertically polarized excitation) for determination of the luminescence lifetime. The fluorescence intensity decay was calculated by fitting the data to a single exponential decay model; here I(t) is the time dependent intensity and I_0 is the intensity at time 0.

$$I(t) = I_0 \exp(-t/\tau) \quad (2)$$

In the time-resolved anisotropy experiment, the depolarization of the emitted light that results from molecular rotation is given by

$$r(t) = \frac{I_{VV(t)} - I_{VH(t)}}{I_{VV(t)} + 2I_{VV(t)}} = \sum_{j=1}^{5} \beta_j e^{-t/\Phi_j} \quad (3)$$

where $I_{VV}(t)$ and $I_{VH}(t)$ represent the vertical and horizontal decays, respectively, obtained using vertical excitation. The pre-exponential factors, β_j, are trigonometric functions of the angles between the excitation and emission transition dipole moments of the probe and the symmetry axes of the ellipsoid of revolution [32], and the sum of β_j is the limiting anisotropy at zero time, r_0, when no motion has occurred. The denominator of Eq. (3) is the total intensity decay, $I(t)$,

$$I_{VV}(t) + 2I_{VH}(t) = I(t) = \sum_{i=1}^{n} \alpha_i e^{-t/\tau_i} \quad (4)$$

where τ_i is the lifetime and α_i is the amplitude of the ith component; the magic angle decay is $I(t)/3$.

The anisotropy decay data were analyzed using the software package FLUOFIT PRO (PicoQuant, Berlin). For anisotropy analysis, the individual vertical and horizontal decays, $I_{VV}(t)$ and $I_{VH}(t)$, respectively, were fit simultaneously according to the following relationships:

$$I_{VV}(t) = G\frac{1}{3}\sum_{i=1}^{n} \alpha_i e^{-t/\tau_i}\left[1 + 2(r_\infty + \sum_{j=1} \beta_j e^{-t/\Phi_j}\right] \quad (5a)$$

$$I_{VH}(t) = \frac{1}{3}\sum_{i=1}^{n} \alpha_i e^{-t/\tau_i}\left[1 - (r_\infty + \sum_{j=1} \beta_j e^{-t/\Phi_j}\right] \quad (5b)$$

where r_∞ is the anisotropy at infinite time [33], and $G = \int I_{HV} dt / \int I_{HH} dt$ is a factor, obtained using horizontal excitation, that corrects for the difference in the efficiencies of the V and H detection channels; under ideal conditions $G \sim 1$ [34,35].

3. Synthesis

The reactive starting complex K[Ru(CF_3CO_2)$_3$(CO)$_3$] (**1**) was synthesized according to the published procedure [23]. Spectroscopic data for the new compounds are summarized in Table 1. Elemental analyses were obtained only for the final diimine complexes. In some cases the lability of the TFA ligand led to elemental analyses slightly out of the required range for carbon content (>0.5%, compounds **7**, **11**, **15**). Mass spectral and spectroscopic data verify identity and purity of these complexes (Table 1).

3.1. Synthesis of [Ru{P(C_6H_5)$_3$}$_2$(CO)$_2$(TFA)$_2$] (**2**), [Ru(η^2(C_6H_5)$_2$PC_2H_4P(C_6H_5)$_2$)(CO)$_2$(TFA)$_2$] (**3**) and [Ru{η^2(C_6H_5)$_2$PC_2H_2P(C_6H_5)$_2$}(CO)$_2$(TFA)$_2$] (**4**)

An acetone solution (30 mL) of K[Ru(CF_3CO_2)$_3$(CO)$_3$] (**1**) (100 mg, 0.18 mmol) and triphenylphosphine (94 mg, 0.36 mmol) was refluxed for 24 h. The solvent was removed by a rotary evaporator and the residue was chromatographed by TLC on silica gel. Elution with hexane/acetone (9:1 v/v) gave two bands. The slower moving band afforded Ru{P(C_6H_5)$_3$}$_2$(CO)$_2$(TFA)$_2$] (**2**) (66 mg, 41%) as a white powder after recrystallization from hexane/acetone at RT.

A mixture of **1** (250 mg, 0.44 mmole) and diphenylphosphinoethane (dppe) (195 mg, 0.48 mmole) was refluxed in an ether–acetone (10 mL/10 mL) solvent for 2 h under N_2. The color of the solution changed from yellow to green. The solvent was removed by a rotary evaporator, taken up into acetone and separated on TLC. Elution with acetone/hexane [1:3 (v/v)] developed two bands. The faster moving yellow band yielded a small amount of **1** and the slower moving green band afforded [Ru(η^2(C_6H_5)$_2$PC_2H_4P(C_6H_5)$_2$)(CO)$_2$(TFA)$_2$] (**3**) (120 mg, 35%).

Reaction of **1** (250 mg, 0.44 mmol) with diphenylphosphinoethylene (194 mg, 0.48 mmol) in refluxing ether–acetone (10 mL/10 mL) solvent followed by similar chromatographic separation afforded [Ru(η^2(C_6H_5)$_2$PC_2H_2P(C_6H_5)$_2$)(CO)$_2$(TFA)$_2$] (**4**) (140 mg, 40%).

3.2. Reaction of [Ru{P(C_6H_5)$_3$}$_2$(CO)$_2$(TFA)$_2$] (**2**) with 1,10-phenanthroline and 2,2′-bipyridyl

The reaction of **2** (100 mg, 0.11 mmole) with 1,10-phenanthroline (40 mg, 0.22 mmole) in refluxing toluene for 72 h resulted in an orange solution. The solvent was removed on a rotary evaporator and the oily residue was dissolved in acetone and placed onto a column of neutral alumina. Elution with hexane/CH_2Cl_2 [3:1 (v/v)] gave two bands. The slower moving orange band gave [Ru{P(C_6H_5)$_3$}$_2$(1,10phenanthroline)(CO)Cl][PF_6] (**5**) (35 mg, 36%) as orange crystals after adding aqueous ammonium hexafluorophosphate and recrystallization from hexane/CH_2Cl_2 (Anal. Calc. for $C_{49}H_{38}O_1P_3F_6Ru_1N_2Cl_1$: C, 58.5; H, 3.83; N, 2.78. Found: C, 58.2; H, 3.62, N, 3.06%). The faster moving yellow band yielded [Ru{P(C_6H_5)$_3$}(1,10-phenanthroline)(CO)(TFA)$_2$] (**6**) (25 mg, 29%) as yellow crystals after re-crystallization from hexane/CH_2Cl_2 (Anal. Calc. for $C_{35}H_{23}N_2P_1O_5F_6Ru_1$: C, 53.77; H, 2.97. Found: C, 54.16; H, 2.78%).

The reaction of **2** (100 mg, 0.11 mmole) with 2,2′-bipyridyl (35 mg, 0.22 mmole) in ethylene glycol (15 mL) at 140 °C for 72 h produced an orange solution. A deep yellow precipitate was obtained by the addition of aqueous NH_4PF_6 (1.0 g/10 mL). The precipitate was dissolved in CH_2Cl_2 and chromatographed on a column of activated alumina (Hexane/CH_2Cl_2, [1:1 v/v]) yielding the compound [Ru{P(C_6H_5)$_3$}$_2$(2,2′-bipyridyl)(CO)TFA][PF_6] (**7**) (48 mg, 47%) as a deep yellow powder (Anal. Calc. for $C_{49}H_{38}O_3P_3F_9Ru_1N_2$: C, 55.44; H, 3.68, N, 2.69. Found: C, 56.06; H, 3.88, N, 3.28%).

Reaction of **2** (210 mg, 0.23 mmol) with 4,4′-dicarboxy-bipyridyl (56 mg, 0.23 mmol) in ethylene glycol (25 mL) at 140 °C for 72 h followed by addition of aqueous NH_4PF_6 (1.0 g/10 mL) resulted in a mixture of [Ru{P(C_6H_5)$_3$}$_2$(4,4′-dicarboxy-bipyridyl)(CO)TFA][PF_6] (**8**) and [HRu{P(C_6H_5)$_3$}$_2$(4,4′-dicarboxy-bipyridyl)(CO)][PF_6] (**9**). Dissolving the mixture in hot ethanol yielded only [HRu{P(C_6H_5)$_3$}$_2$(4,4′-dicarboxy-bipyridyl)(CO)][PF_6] (**9**) (102 mg, 54%) (Anal. Calc. for $C_{49}H_{39}O_5P_3F_6Ru_1N_2$: C, 56.38; H, 3.77, N, 2.69. Found: C, 57.1; H, 3.88, N, 2.62%).

Re-crystallization of **7** from hot ethanol gave pale yellow crystals of [HRu{P(C_6H_5)$_3$}$_2$(2,2′-bipyridyl)(CO)][PF_6] (**10**).

3.3. Reaction of of [Ru{η^2(C_6H_5)$_2$PC_2H_4P(C_6H_5)$_2$}(CO)$_2$(TFA)$_2$] (**3**) with 1,10-phenanthroline and 2,2′-bipyridyl

Compound **3** (120 mg, 0.153 mmole) was heated with 1,10-phenanthroline (83 mg, 0.461mmole) in ethylene glycol (15 mL) at 140 °C for 72 h, The color of the reaction mixture turned to deep orange. An orange precipitate of [(CO)(TFA)Ru{η^2(C_6H_5)$_2$PC_2H_4P(C_6H_5)$_2$}($\eta^2C_{12}H_8N_2$)][PF_6] (**11**) (84 mg, 56%) was obtained by adding aqueous NH_4PF_6 (1.0 g/10 mL) to the reaction mixture. The residue was then filtered and washed tree times with DI water and three times with diethyl ether and dried under vacuum (Anal. Calc. for $C_{41}H_{32}O_3P_3F_9Ru_1N_2$: C, 51.0; H, 3.33, N, 2.91. Found: C, 51.9; H, 3.65, N, 3.21%).

A similar reaction of compound **2** (120 mg, 0.153 mmole) with 2,2′-bipyridyl (71 mg, 0.46 mmole) in ethylene glycol (15 mL) at 140 °C for 72 h followed by addition of aqueous NH_4PF_6 (1.0 g/10 mL) gave [(CO)(TFA)Ru{η^2(C_6H_5)$_2$PC_2H_4P(C_6H_5)$_2$}($\eta^2C_{10}H_8N_2$)][PF_6] (**12**) (80 mg, 55%) (Anal. Calc. for $C_{39}H_{32}O_3P_3F_9Ru_1N_2$: C, 49.7; H, 3.41. Found: C, 50.1; H, 3.72%).

3.4. Reaction of of [Ru{η^2(C_6H_5)$_2$PC_2H_2P(C_6H_5)$_2$}(CO)$_2$(TFA)$_2$] (**4**) with 1,10-phenanthroline, 2,2′-bipyridyl and 5-amino-1,10-phenanthroline

A mixture of **4** (130 mg, 0.167 mmole) and 1,10-phenanthroline (86 mg, 0.48 mmole) in ethylene glycol (15 mL) was heated at 140 °C for 72 h. Addition of aqueous NH_4PF_6 (1.0 g/10 mL) to the reaction mixture yielded the yellow precipitate of [(CO)(TFA)Ru{η^2(C_6H_5)$_2$PC_2H_2P(C_6H_5)$_2$}(η-$^2C_{12}H_8N_2$)][PF_6] (**13**) (95 mg, 59%). The residue was then filtered and washed tree times with DI water and three times with diethyl ether and dried under vacuum (Anal. Calc. for $C_{41}H_{30}O_3P_3F_9Ru_1N_2$: C, 51.1; H, 3.11. Found: C, 51.6; H, 2.97%).

A similar reaction of compound **4** (140 mg, 0.18 mmole) with 2,2′-bipyridyl (71 mg, 0.46 mmole) in ethylene glycol (15 mL) at 140 °C for 72 h followed by addition of aqueous NH_4PF_6 (1.0 g/10 mL) afforded [(CO)(TFA)Ru{η^2(C_6H_5)$_2$PC_2H_4P(C_6H_5)$_2$}($\eta^2C_{10}H_8$ N_2)][PF_6] **14** (65 mg, 45%) (Anal. Calc. for $C_{39}H_{30}O_3P_3F_9Ru_1N_2$: C, 49.89; H, 3.19. Found: C, 50.26; H, 3.42%).

The reaction of compound **4** (140 mg, 0.18 mmole) with 5-amino-1,10-phenanthroline (39 mg, 0.19 mmole) in ethylene glycol (15 mL) at 140 °C for 72 h followed by addition of aqueous NH_4PF_6 (1.0 g/10 mL) and purification on an activated alumina column (elution with CH_2Cl_2/MeCN, [2:1 v/v]) gave [(CO)Ru({η^2(C_6H_5)$_2$ PC_2H_2P(C_6H_5)$_2$}TFA($\eta^2C_{10}H_9N_3$)][PF_6] (**15**) (80 mg, 55%). It was not possible to obtain good elemental analysis for this compound probably owing to the lability of the TFA.

The addition of conc. Hydrochloric acid or aqueous NaCl to a methanol solution of **15** afforded hydride complex [HRu({η^2(C_6H_5)$_2$PC_2H_4P(C_6H_5)$_2$}(CO)($\eta^2C_{10}H_9N_3$)][PF_6] (**16**). The mass spectra showed trace of the chloride product [ClRu({η^2(C_6H_5)$_2$PC_2H_4P(C_6H_5)$_2$}(CO)($\eta^2C_{10}H_9N_3$)][PF_6] present with the hydride complex. ESI-MS: *m*/*z* 924 [M+Na] (Calc. M = 902).

4. Results and discussion

4.1. Compound synthesis and reaction pathways

The phosphine complexes $[Ru\{P(C_6H_5)_3\}_2(CO)_2(TFA)_2]$ (**2**), $[Ru(\eta^2(C_6H_5)_2PC_2H_4P(C_6H_5)_2)(CO)_2(TFA)_2]$ (**3**) and $[Ru\{\eta^2(C_6H_5)_2PC_2H_2P(C_6H_5)_2\}(CO)_2(TFA)_2]$ (**4**) were prepared (Scheme 1), and a series of stepwise reactions shown in Schemes 2–7 show the preparation of the luminescent ruthenium MLC complexes of formula [XRu(CO)(diimine)$(L)_2$][PF_6] as well as the non-luminescent [$(TFA)_2$Ru(CO)(2,2′-bpy)(PPh_3)]. The stepwise carbonyl and TFA (TFA = trifluoroacetate) ligand replacement reactions were monitored by IR and ^{31}PNMR spectroscopic methods.

The Reaction of **2** with 1,10-phenanthroline in refluxing toluene for 72 h followed by chromatographic separation with an alumina column and crystallization from CH_2Cl_2/hexane yielded [Ru{$P(C_6H_5)_3$}$_2$(1,10-phenanthroline)(CO)Cl][PF_6] (**5**) and [Ru{$P(C_6H_5)_3$}(1,10-phenanthroline)(CO)($(TFA)_2$] (**6**) in 36% and 29% yields, respectively (Scheme 2). The reaction of Compound **2** with 2,2′-bipyridyl or 4,4′-dicarboxy-2,2′-bipyridyl in ethylene glycol at 140 °C gave [Ru{$P(C_6H_5)_3$}$_2$(2,2′-bipyridyl)(CO)TFA][PF_6] (**7**) and [Ru{$P(C_6H_5)_3$}$_2$(4,4′-dicarboxy-bipyridyl)(CO)TFA][PF_6] (**8**) with a small amount of [HRu{$P(C_6H_5)_3$}$_2$(4,4′-dicarboxybipyridyl)(CO)][PF_6] (**9**), respectively. Crystallization of **7** and the mixture of **8** and **9** from hot ethanol yielded only the hydride complexes as [HRu{$P(C_6H_5)_3$}$_2$(2,2′-bipyridyl)(CO)][PF_6] (**10**) and [HRu{$P(C_6H_5)_3$}$_2$(4,4′-dicarboxy-bipyridyl)(CO)][PF_6] (**9**), respectively (Scheme 3). All these complexes were characterized by elemental analysis, infrared, ^{1}H NMR, ^{31}P–{^{1}H} NMR, UV–Vis and mass spectral data (Table 1). The structure of the complexes **5**, **6** and **10** was further investigated by single crystal X-ray diffraction analysis.

Complex **7** contains the labile ligand TFA (trifluoroacetate) *trans* to the N of the bipyridyl ligand. In solution, the complex can lose the TFA ligand to form the trigonal–bipyramidal intermediate with a vacant coordination site. Coordinative solvents like alcohols can coordinate to the vacant site *trans* to the N of the bipyridyl ligand, which then undergoes ejection of a proton to form a methoxide complex, and then β-elimination to give the hydride complex. A proposed mechanism for hydride formation is shown in Scheme 4.

4.1.1. Reaction of the chelating phosphine complexes with the diimine ligands

The reactions of complex **3** with 1,10-phenanthroline or 2,2′-bipyridyl in ethylene glycol formed [(CO)(TFA)Ru{$\eta^2(C_6H_5)_2PC_2H_4P(C_6H_5)_2$}($\eta^2C_{12}H_8N_2$)][$PF_6$] (**11**) and [(CO)(TFA)Ru{$\eta^2(C_6H_5)_2PC_2H_4P(C_6H_5)_2$}($\eta^2C_{10}H_8N_2$)][$PF_6$] (**12**) in 56% and 55% yield, respectively (Scheme 5). Similarly, heating complex **4** with 1,10-phenanthroline or 2,2′-bipyridyl in ethylene glycol at 140 °C afforded [(CO)(TFA)Ru{$\eta^2(C_6H_5)_2PC_2H_2P(C_6H_5)_2$}($\eta^2C_{12}H_8$ N_2)][PF_6] (**13**) and [(CO)(TFA)Ru{$\eta^2(C_6H_5)_2$ $PC_2H_4P(C_6H_5)_2$}-($\eta^2C_{10}H_8N_2$)][PF_6] (**14**) in 59% and 45% yields, respectively (Scheme 6). Reaction of **4** with bio-conjugable ligand 5-amino-1,10-phenanthroline in ethylene glycol at 140 °C gave [(CO)Ru({$\eta^2(C_6H_5)_2PC_2H_4$-$P(C_6H_5)_2$}TFA($\eta^2C_{10}H_9N_3$)] [PF_6] (**15**) in 55% yield (Scheme 6).

All these complexes were characterized by elemental analysis, infrared, ^{1}H NMR, ^{31}P–{^{1}H} NMR, UV–Vis and mass spectral data (Table 1). Due to the presence of the labile ligand TFA, these complexes are unstable in solution, and we were not able to obtain good quality crystals for X-ray crystallographic analysis. Addition of Conc. HCl or aqueous NaCl solution to the methanol solution of **15** produced complex [HRu({$\eta^2(C_6H_5)_2PC_2H_4P(C_6H_5)_2$}(CO)($\eta^2C_{10}H_9N_3$)][$PF_6$] (**16**) along with trace amount of [Ru{$\eta^2(C_6H_5)_2PC_2H_4P(C_6H_5)_2$}(CO)($\eta^2C_{10}H_9N_3$)Cl][$PF_6$]. The ESI-MS gave an m/z = 924, due to formation of the Na^+ adduct, shows the presence of this compound as a mixture with the hydride compound (Scheme 7). The hydride complex was confirmed by the observed pentaplet at −7.4. A probable route to hydride formation in the H_2O/MeOH solution is shown in Scheme 8. There is a possibility that the reaction with HCl and NaCl is catalyzed by the H^+ present in the solution. It is predicted that the complex **15** loses the labile ligand, TFA, followed by the coordination of H_2O. Protonation of this bound water molecule then facilitates hydride transfer to the metal center.

4.2. Solid state structures of compounds *5*, *6* and *10*

The solid state structures of **5**, **6** and **10** are shown in Fig. 1, crystal data are given in Table 2 and selected distances and angles are given in Tables 3–5. Complexes **5** and **10** contain two mono-dentate triphenylphosphine ligands *trans* to each other and complex

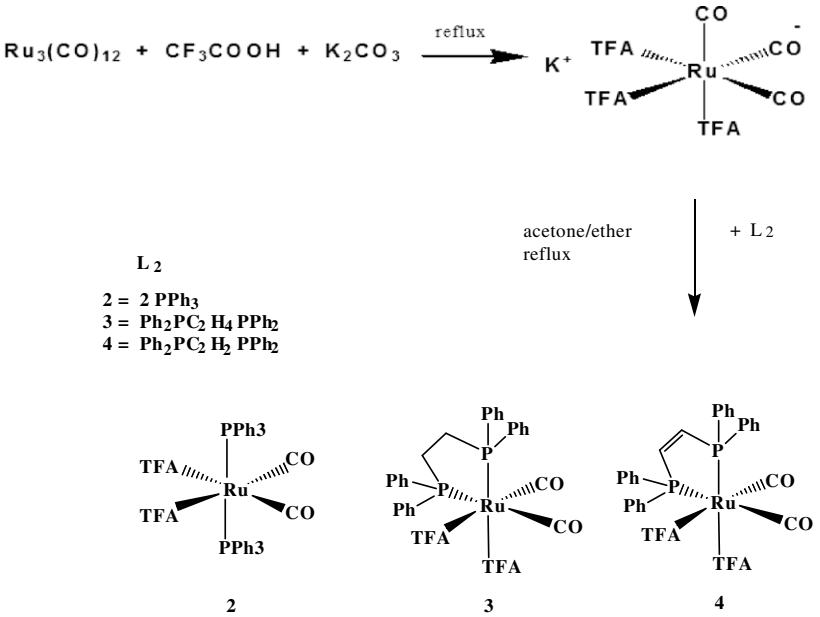

Scheme 1.

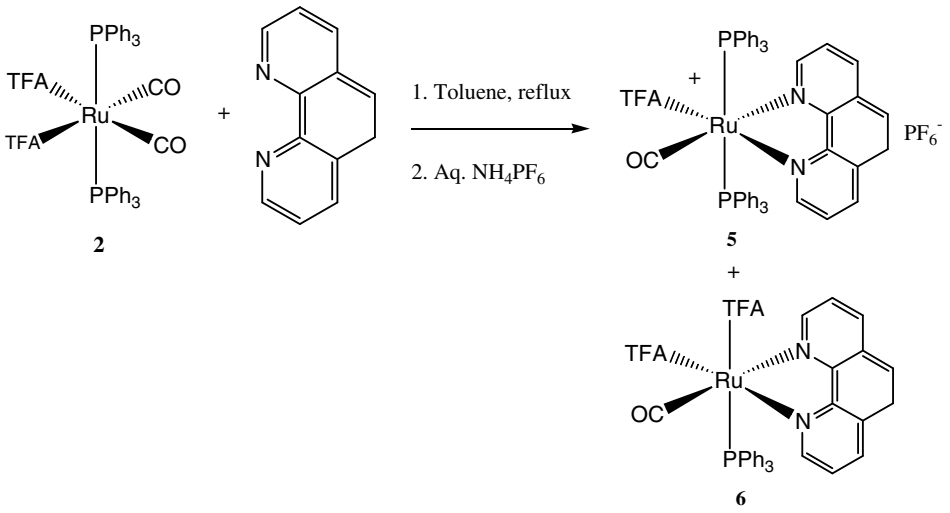

Scheme 2.

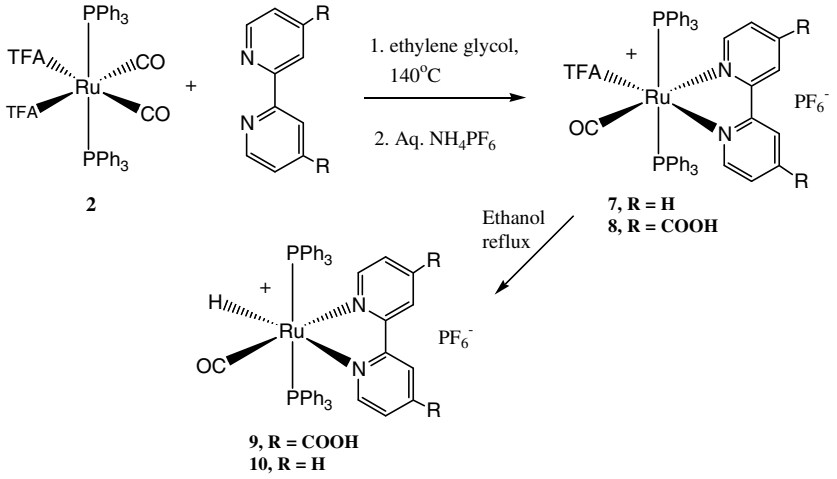

Scheme 3.

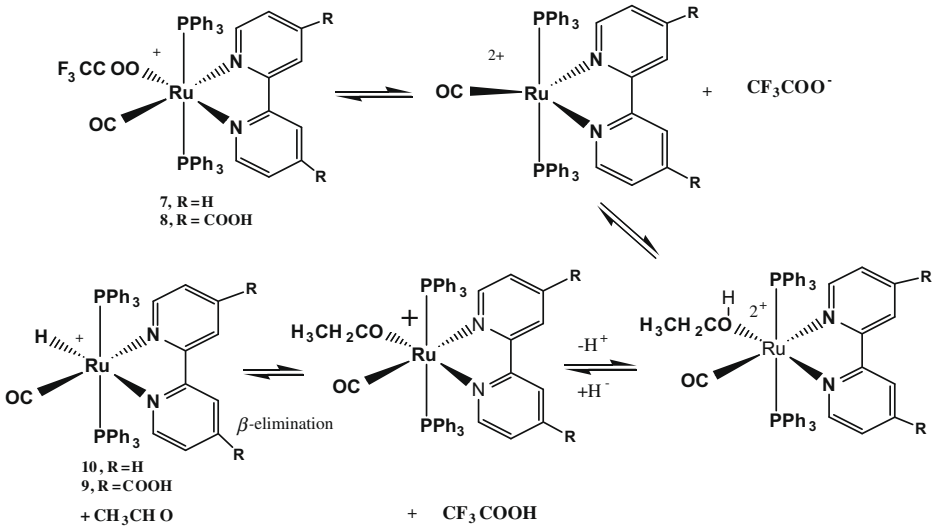

Scheme 4.

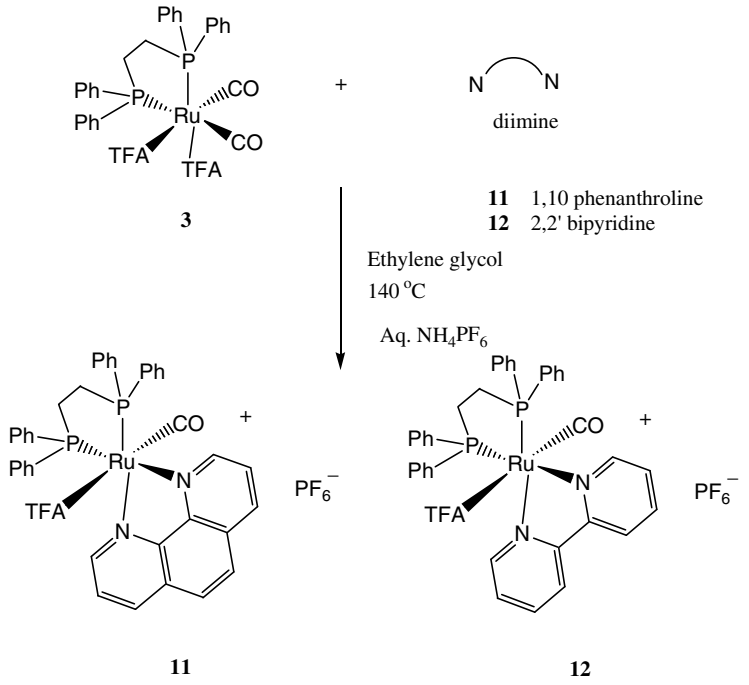

Scheme 5.

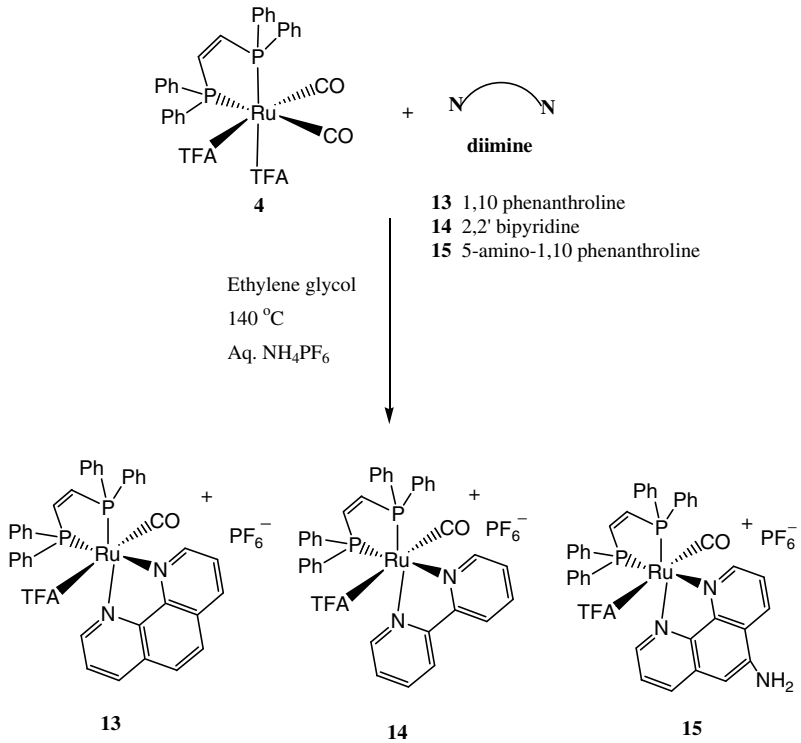

Scheme 6.

6 contains only one triphenylphosphine ligand. The presence of $[PF_6]$ anion assures the positive charge on **5** and **10** whereas complex **6** is a neutral complex as it contains two TFA ligands *cis* with respect to each other.

The ligands in these complexes are arranged in close to octahedral geometry around the Ru atom. The chelating bi-dentate diimine ligands in **5**, **6** and **10** are bound to the Ru(II) with a bite angle 78.19(13), 79.2(13) and 74.5(17)°, respectively. This structural feature is similar to other Ru–diimine complexes [23,36]. The Ru–N phenanthroline (2.06–2.13 Å) and Ru–N bipyridine (2.10–2.16 Å) bond lengths of the coordinated diimine ligands are also comparable to those observed in other Ru–diimine complexes [36]. All these complexes contain one carbonyl ligand attached to the metal center and the Ru–C bond lengths of **5**, **6** and **10** [1.866(9), 1.864(4) and 1.816(15) Å] are similar to those observed for similar Os and Re complexes [36–38]. The exchange of Cl for

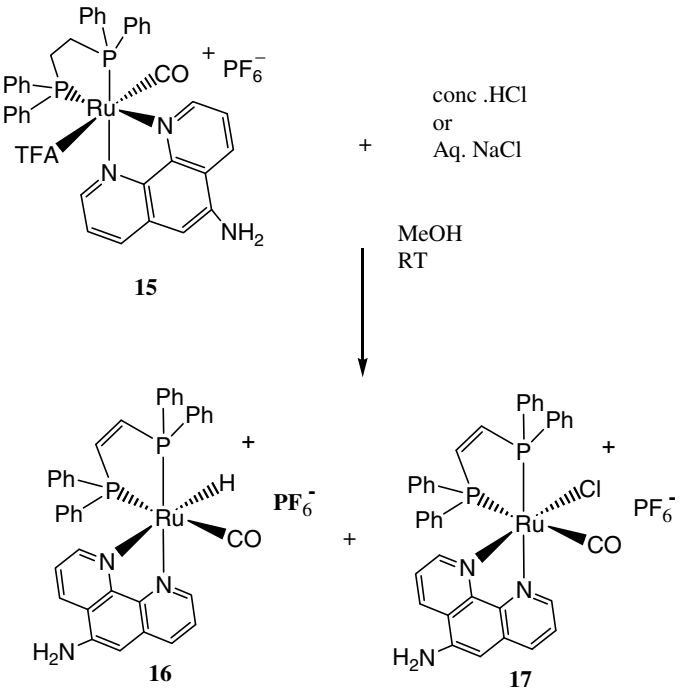

Scheme 7.

TFA ligand in complex **5** resulted in disordering of the CO and Cl ligands. The hydride ligand in the equatorial position of complex **10** is *trans* to N(2) of the bipyridine ligand and Ru–H bond length is 2.04(5). The presence of this hydride was confirmed by ^{1}H NMR.

4.3. Spectroscopic characterization

4.3.1. Infrared spectral analysis

The infrared spectra of the metal bound carbonyl stretching region (ν_{CO}) provided important information about the stepwise ligand substitutions performed on the precursor **1**. All of the complexes synthesized contain metal-coordinated carbonyl ligands. M–CO shows CO stretching modes around 2150–1750 cm^{-1}, which are easily distinguishable from organic CO frequencies. The M–CO signals are very sensitive to the electronic properties of the other ligands present on the metal. The observed changes in the carbonyl stretching region are due to the replacement of CO ligands by phosphines and diimine ligands, respectively. Introduction of electron rich ligands such as Ph_3P, dppe and dppene decreased the energy of the M-CO bands. Phosphine compounds **2**–**4** showed two strong M–CO stretches at 2066 and 2002 cm^{-1}, confirming that they are di-carbonyl complexes; the strong ν_{CO} at 1696 cm^{-1} is due to the two CF_3COO^- ligands. The complexes **5**–**16** have only one M–CO ligand, and usually the strong M–CO stretch appears at 1995–1985 cm^{-1} for the non-hydride complexes. Replacement of CF_3COO^- by the more electron-donating hydride ligand shifts ν_{CO} to lower energy in complexes **9**, **10** and **16**. A strong absorption at 1734 cm^{-1} was also observed for the carboxyl groups of 4,4′-dicarboxy-2,2-bipyridyl of **8** and **9**. Raman spectra of the metal hydrides show characteristic ν_{M-H} stretches at 1800–2000 cm^{-1} [39]. Raman spectra of complexes **9** and **10** have ν_{M-H} at 1920 and 1950 cm^{-1}, respectively.

4.3.2. NMR spectral analysis

The ^{1}H and ^{31}P NMR spectra of these complexes obtained in acetone d^6 are consistent with the predicted structures. NMR spectral analysis was an important tool to assign the presence of the terminal hydride ligand in the complexes **9**, **10** and **15**. The aromatic region of the ^{1}H spectra is complex due to presence of phenyl protons of phosphines ligands and the aromatic protons of diimine ligands. The chemical shifts and coupling constants are listed in Table 1. The phenyl protons of PPh_3 (complexes **2** and **5**–**10**) and chelating phosphines (complexes **3**, **4** and **11**–**16**) appear as multiplets at δ 7.2–7.6 ppm. The CH=CH protons of diphenylphosphinoethylene are observed around δ 6.4–6.9 ppm and the alkyl protons of diphenylphosphinoethane are observed around δ 2.03–3.6 ppm. The M–H resonance appears as a triplet at δ −11.09 (J = 20 Hz) and −11.07 (J = 20 Hz) for complexes **9** and **10**, respectively. In the case of complex **16**, the pentuplet is observed at δ −7.7 ppm (J = 20 Hz).

The ^{31}P NMR spectra greatly facilitated structural characterization of these complexes. The chemical shift of the metal bound phosphines ligands are in good agreement with the similar Ru(II)

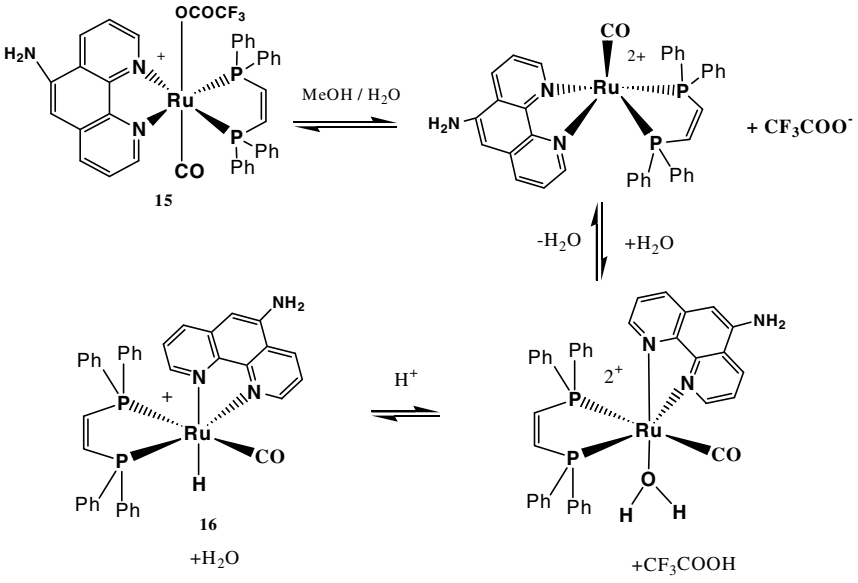

Scheme 8.

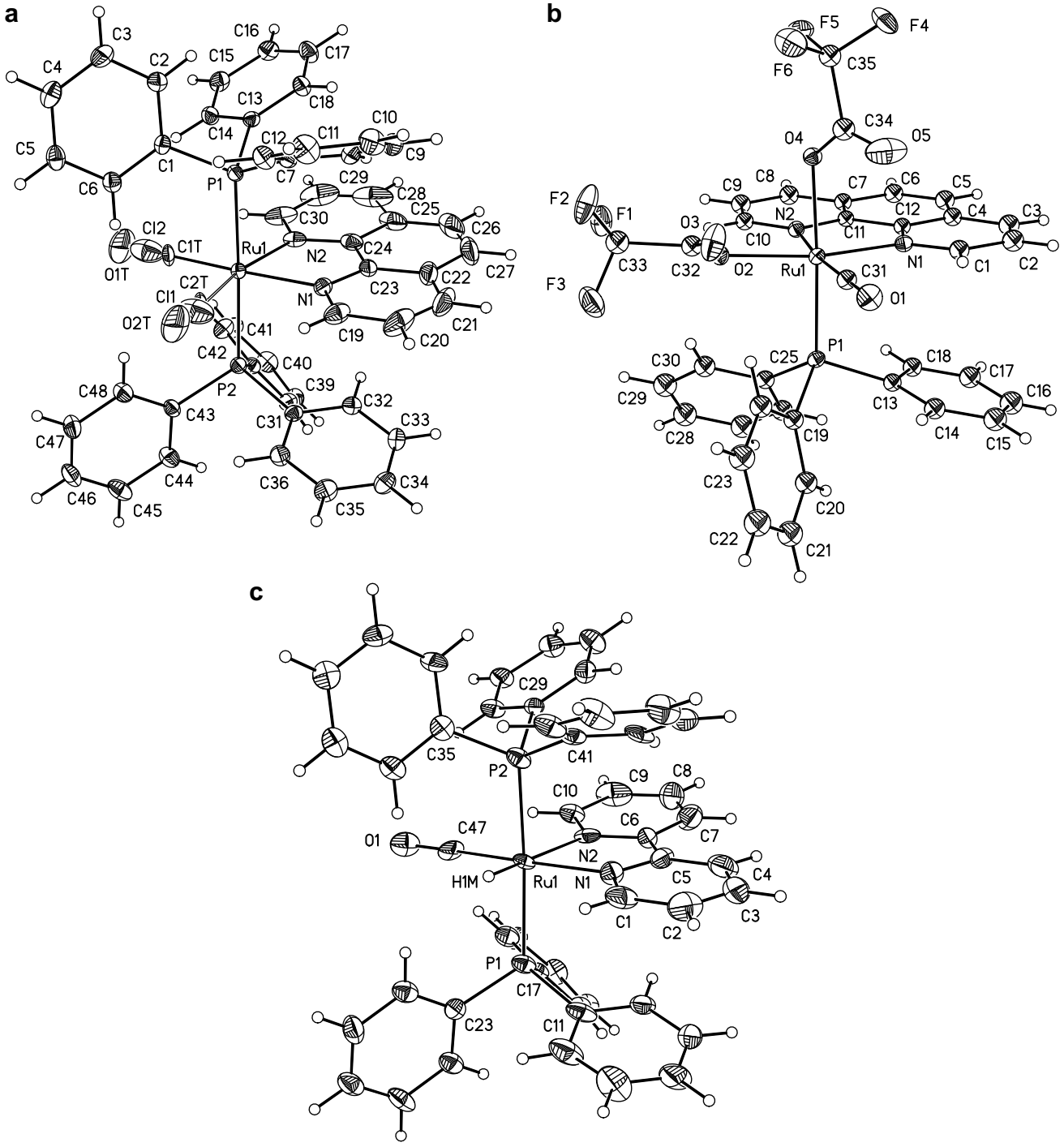

Fig. 1. Solid state structure of (a) $C_{49}H_{38}C_lF_6N_3O_4P_3Ru_1$ (**5**), (b) $C_{35}H_{23}F_6N_2O_5P_1Ru_1$ (**6**) and (c) $C_{47}H_{39}F_6N_2O_1P_3Ru_1$ (**10**) showing the 90% probability thermal elipsoids and the calculated positions of the hydride and hydrogen atoms.

phosphine complexes. Complexes **2**, **5**, **6** and **7** show singlet resonances at 26–30 ppm, relative to external H_3PO_4, due to the PPh_3 ligands. The sharp singlet observed for these complexes (**2**, **5** and **7**) indicated that the two phosphorous nuclei are magnetically equivalent, and therefore are *trans* to each other. In the chelating phosphine complexes, the two phosphorous nuclei must be *cis* to each other and therefore two singlets at 45.8 and 45.07 ppm for complex **3** and at 53.9 and 53.4 ppm for complex **4** are observed. The ^{31}P–^{31}P coupling is apparently small in these complexes. The observation of two resonances in the ^{31}P NMR for **3** and **4** requires that one of the two remaining CO ligands and one of the two remaining TFA ligands are trans to each phosphorous. Otherwise the molecule would have a plane of symmetry and one ^{31}P NMR resonance would be observed. However, when the diimine ligand is introduced, only one sharp signal for the chelating phosphine ligand is observed. This indicates that complexes **11**–**16** have a symmetry component that makes the two phosphorous nuclei equivalent (Schemes 2, 3 and 5). With the exception of complex **6**, complexes **5**–**16** all contain $[PF_6]$ as a counter ion, which appeared in the ^{31}P NMR as a septet at −155 ppm with an integrated

Table 2
Summary of crystal data and structure refinement for compound **5**, **6** and **10**.

Compound	**5**	**6**	**10**
Empirical formula	$C_{49}H_{38}ClF_6N_3O_4P_3Ru$	$C_{35}H_{23}F_6N_2O_5PRu$	$C_{47}H_{39}F_6N_2OP_3Ru$
Formula weight	1076.25	797.59	955.78
Temperature (K)	173(2)	173(2)	173(2)
Wavelength (Å)	0.71073	1.54178	0.71073
Crystal system	Triclinic	Monoclinic	Triclinic
Space group	$P\bar{1}$	$P_2(1)/n$	$P\bar{1}$
Unit cell dimensions			
a (Å)	12.0192(8)	11.0644(2)	11.848(3)
b (Å)	13.8790(9)	20.2377(4)	13.558(3)
c (Å)	14.7094(9)	15.1820(3)	14.869(4)
α (°)	92.1380(10)	90	89.908(4)
β (°)	99.2250(10)	93.896	81.975(4)
γ (°)	103.3140(10)	90	79.685(4)
Volume (Å^3)	2349.9(3)	3391.67(11)	2326.2(9)
Z	2	4	2
D_{calc} (Mg/m^3)	1.521	1.562	1.365
Absorption coefficient (mm^{-1})	0.565	4.882	0.500
$F(000)$	1090	1600	972
Crystal size (mm^3)	0.285 × 0.235 × 0.133	0.35 × 0.15 × 0.15	0.19 × 0.12 × 0.12
θ Range for data collection (°)	1.41–28.37	3.64–66.38	1.76–23.82
Index ranges	$-16 \ll h \ll 16$, $-18 \ll k \ll 18$, $-19 \ll l \ll 19$	$-12 \ll h \ll 13$, $-23 \ll k \ll 23$, $-17 \ll l \ll 17$	$-13 \ll h \ll 13$, $-15 \ll k \ll 15$, $-16 \ll l \ll 16$
Reflections collected	34911	19108	20092
Independent reflections [R_{int}]	11720 [0.0373]	5716 [0.0237]	13496 [0.0668]
Completeness to θ = 66.38°	99.5%	95.9%	100.0%
Data/restraints/parameters	11720/2/614	5716/0/279	13496/3/358
Goodness-of-fit on F^2	1.154	1.069	1.082
Final R indices [$I > 2\sigma(I)$]	R_1 = 0.0619, wR_2 = 0.1487	R_1 = 0.0432, wR_2 = 0.1350	R_1 = 0.0877, wR_2 = 0.1852
R indices (all data)	R_1 = 0.0701, wR_2 = 0.1532	R_1 = 0.0453, wR_2 = 0.1368	R_1 = 0.1300, wR_2 = 0.2079
Largest difference peak and hole (e Å^{-3})	1.112 and −2.227	2.196 and −0.512	1.223 and −1.916

Table 3
Selected bond distances (Å) and angles (°) for $C_{49}H_{38}C_lF_6N_2OP_3Ru_1$ (**5**).

N(1)–Ru(1)	2.110(3)	C(1T)–O(1T)	1.222(8)
N(2)–Ru(1)	2.127(3)	C(1T)–Ru(1)	1.866(9)
P(1)–Ru(1)	2.3732(9)	C(2T)–O(2T)	1.193(8)
P(2)–Ru(1)	2.3782(9)	C(2T)–Ru(1)	1.891(11)
Cl(2)–Ru(1)	2.480(5)	Cl(1)–Ru(1)	2.475(3)
C(1T)–Ru(1)–C(2T)	93.3(6)	C(1T)–Ru(1)–N(1)	177.1(4)
C(2T)–Ru(1)–N(1)	89.5(3)	C(1T)–Ru(1)–N(2)	99.0(4)
C(2T)–Ru(1)–N(2)	167.7(3)	N(1)–Ru(1)–N(2)	78.19(13)
C(1T)–Ru(1)–P(1)	88.7(3)	C(2T)–Ru(1)–P(1)	90.7(3)
N(1)–Ru(1)–P(1)	90.89(8)	N(2)–Ru(1)–P(1)	88.99(8)
C(1T)–Ru(1)–P(2)	90.3(3)	C(2T)–Ru(1)–P(2)	87.5(3)
N(1)–Ru(1)–P(2)	90.28(8)	N(2)–Ru(1)–P(2)	92.98(8)
P(1)–Ru(1)–P(2)	177.88(3)	C(1T)–Ru(1)–Cl(1)	97.5(4)
C(2T)–Ru(1)–Cl(1)	4.9(4)	N(1)–Ru(1)–Cl(1)	85.32(15)
N(2)–Ru(1)–Cl(1)	163.22(15)	P(1)–Ru(1)–Cl(1)	88.20(9)
P(2)–Ru(1)–Cl(1)	90.14(9)	C(1T)–Ru(1)–Cl(2)	1.6(5)
C(2T)–Ru(1)–Cl(2)	94.6(3)	N(1)–Ru(1)–Cl(2)	175.81(12)
N(2)–Ru(1)–Cl(2)	97.66(12)	P(1)–Ru(1)–Cl(2)	89.61(8)
P(2)–Ru(1)–Cl(2)	89.36(8)	Cl(1)–Ru(1)–Cl(2)	98.86(16)

Table 4
Selected bond distances (Å) and angles (°) for $C_{35}H_{23}F_6N_2O_5P_1Ru_1$ (**6**).

N(1)–Ru(1)	2.062(3)	C(31)–O(1)	1.145(5)
N(2)–Ru(1)	2.133(3)	C(31)–Ru(1)	1.864(4)
O(2)–Ru(1)	2.086(3)	P(1)–Ru(1)	2.3020(10)
O(4)–Ru(1)	2.148(3)		
C(31)–Ru(1)–N(1)	93.95(16)	C(31)–Ru(1)–O(4)	95.47(15)
C(31)–Ru(1)–O(2)	99.28(15)	N(1)–Ru(1)–O(4)	88.54(12)
N(1)–Ru(1)–O(2)	165.79(12)	O(2)–Ru(1)–O(4)	85.08(11)
C(31)–Ru(1)–N(2)	173.27(15)	N(2)–Ru(1)–O(4)	83.44(11)
N(1)–Ru(1)–N(2)	79.40(13)	C(31)–Ru(1)–P(1)	88.53(13)
O(2)–Ru(1)–N(2)	87.25(12)		

relative intensity of 1:2 when compared with the phosphine ligand resonances.

4.4. Electrochemistry

The redox properties of the series of Ru carbonyl complexes (**7**, **9**, **10**, **13**, **14** and **15**) were determined by cyclic voltammetry. The cyclic voltammetric (CV) responses are, generally speaking, not well resolved and have as many as four ill-defined peaks.

In the bipyridyl-based complexes (**7**, **9** and **10**), a series of four redox steps are observed. It is likely that both metal- and ligand-centered reductions occur, but it is not possible to discriminate them on the basis of the obtained CVs. As an example, we show in Fig. 2 the cyclic voltammetric (CV) response on a glassy carbon electrode (GC) of a CH_2Cl_2/0.1 M $[NBu_4]PF_6$ solution of **7** at a 0.2 V s^{-1} scan rate (v). Apparently, only the first peak couple ($E^{o\prime}$ (A/A') = −1.02 V vs. SCE) is chemically reversible, although the second and the third ($E_{p,c}$ (B) = −1.76 V, and $E_{p,c}$ (C) = −2.06 V vs. Fc/Fc$^+$, respectively) show a hint of a return peak in the reverse scan, in particular when the fourth peak ($E_{p,c}$ = (D) −2.30 V vs. Fc/Fc$^+$) is not traversed. The other complexes of the series show similar behavior and number of peaks. Changing the scan rates to 0.5 and 1.0 V s^{-1} did not significantly change the appearance of the voltammograms.

Table 5
Selected bond distances (Å) and angles (°) for $C_{47}H_{39}F_6N_2O_1P_3Ru_1$ (**10**).

N(1)–Ru(1)	2.102(6)	C(47)–O(1)	1.151(18)
N(2)–Ru(1)	2.163(6)	C(47)–Ru(1)	1.816(15)
P(1)–Ru(1)	2.347(5)	P(2)–Ru(1)	2.349(5)
Ru(1)–H(1)	2.040(5)		
O(1)–C(47)–Ru(1)	174.5(14)	C(47)–Ru(1)–N(1)	179.2(5)
C(47)–Ru(1)–N(2)	105.1(5)	N(1)–Ru(1)–N(2)	74.20(17)
C(47)–Ru(1)–P(1)	88.9(5)	N(1)–Ru(1)–P(1)	91.0(2)
N(2)–Ru(1)–P(1)	94.7(2)	C(47)–Ru(1)–P(2)	90.7(5)
N(1)–Ru(1)–P(2)	89.5(2)	N(2)–Ru(1)–P(2)	90.4(2)
P(1)–Ru(1)–P(2)	174.8(2)	C(47)–Ru(1)–H(1)	99.8
N(1)–Ru(1)–H(1)	81.0	N(2)–Ru(1)–H(1)	155.0
P(1)–Ru(1)–H(1)	82.5	P(2)–Ru(1)–H(1)	92.4

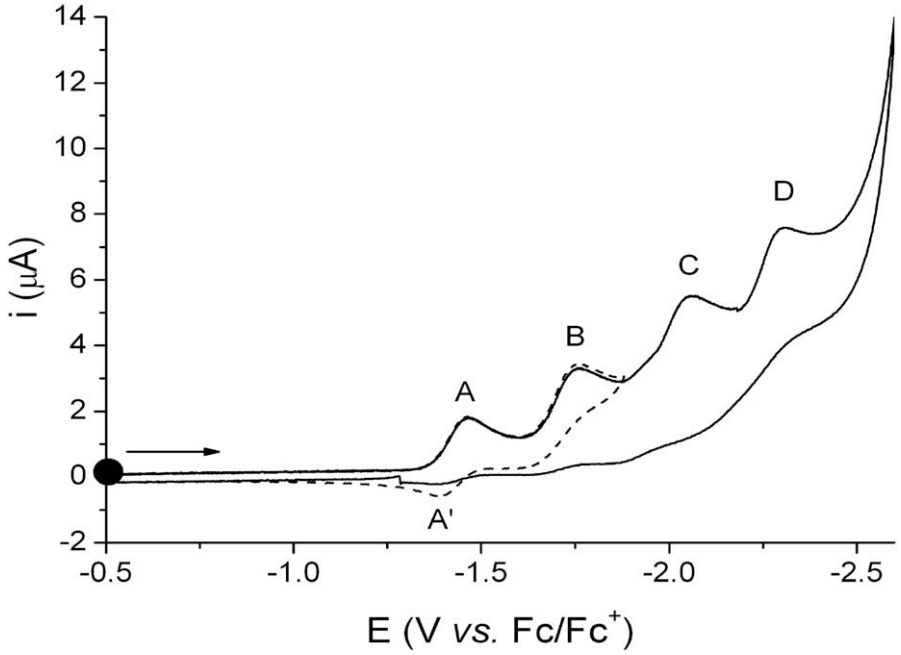

Fig. 2. CV of a 1.0 mM solution of 7 in CH_2Cl_2 containing 0.10 M $[NBu_4][PF_6]$, at a GC working electrode; $v = 0.2$ V s^{-1} (● starting potential).

The phenanthroline-based series of complexes exhibit considerable overlap of the observed redox wave CVs. Only complex **5** shows three well-resolved, chemically and electrochemically reversible, redox steps: two reductions ($E^{o\prime}$ (E/E') = −1.70, and $E^{o\prime}$ (F/F') = −1.93 V vs. Fc/Fc^+, respectively), accompanied by an oxidation in the positive scan ($E^{o\prime}$ (G/G') = +1.04 V vs. Fc/Fc^+) (Fig. 3). The closely related **7** does not show this reversible oxidation, probably owing to the differences between the electronic properties between the phenanthroline and bipyridyl ligands.

A reasonable interpretation of the multiple redox couples observed for complexes **5** and **7** is that the first reduction is the Ru(II) to Ru(I) couple, while the complex and more negative potentials are the result of electron donation to the diimine ligand and/or the phenyl rings on the phosphine ligands [40]. There is considerable precedent for such multiple electron transfers to diimine ligands in related Ru(II) complexes [40]. However, we cannot differentiate at this time whether the CO and phosphine ligands are also participating as electron acceptors. The different reduction potentials and the different degrees of redox-wave-overlap are consistent with this interpretation. The observation of a reversible oxidation wave for complex **5** makes this complex a good candidate for electrochemiluminescence studies.

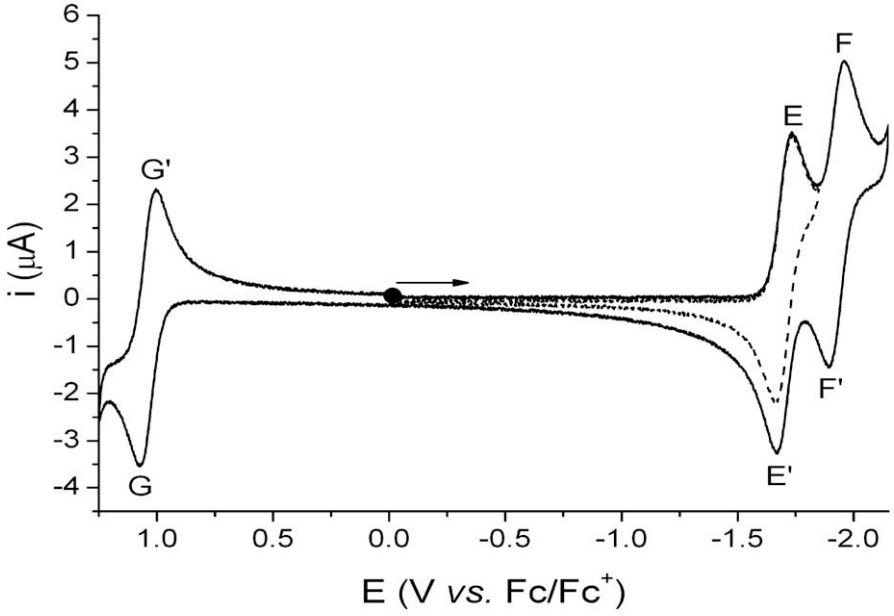

Fig. 3. CV of a 1.0 mM solution of **5** in CH_2Cl_2 containing 0.10 M $[NBu_4][PF_6]$, at a GC working electrode; $v = 0.2$ V s^{-1} (● starting potential).

Table 6
UV–Vis absorption and emission data for **5**–**7** and **9**–**15**.

Compound	λ_{abs} MLCT(nm)	$\lambda_{Excitation}$ (nm)	λ_{E}m (nm)	Φ[a]	τ (ns)
5	420[b]	425	595[b]	0.08	110 (330)[b,c]
6	410[b]	410	–	–	–
7	420[b]	425	611[b]	0.12	185 (680)[b,c]
9	450	450	647	0.30	720 (2630)[c]
10	445	450	607	0.11	847
11	445[b]	450	590[b]	0.12	106 (325)[c]
12	450[b]	450	610[b]	0.08	180
13	440[b]	450	590[b]	0.09	126
14	445	450	610	0.07	190
15	450	470	607	0.25	250 (570)[c]

The photophysical studies were done making solution in acetonitrile and ethanol.
[a] Referenced to 0.73 Quinine disulfate in H_2SO_4 (dilute) (31). Estimated error in relative yields is nearly 15%. Rhodamine emission is in the same region as the MLCT transition.
[b] Solvent was acetonitrile.
[c] The lifetime was recorded after exclusion of oxygen by purging Ar for 30 min in ethanol solution. The MLCT absorptions are broad.

The other compounds in the series also show complex electrochemical behavior, preventing meaningful tabulation of the electrochemical parameters.

4.5. Photophysical properties of *5*–*16*

4.5.1. Absorption spectra

The UV–Vis absorption spectra of the synthesized complexes **5**–**15** were measured at room temperature in ethanol and/or acetonitrile solution (Table 6). The absorption spectra were also recorded in water for complexes **10** and **15**, as both of these complexes have bio-conjugable functional groups. The ruthenium complexes $[(CO)LRu(diimine)(L_2)][PF_6]$ have six d electrons in the three t_2 orbitals, and the diimine ligand provides low-energy π^* orbitals that upon excitation can accept an electron from the electron-rich metal center. Consequently, these complexes display weak absorption bands around 400–500 nm due to the singlet metal-to-ligand charge-transfer (^{1}MLCT) [5]. The strong absorption bands below 390 nm are assigned to intra-ligand charge-transfer (π–π and n–π).

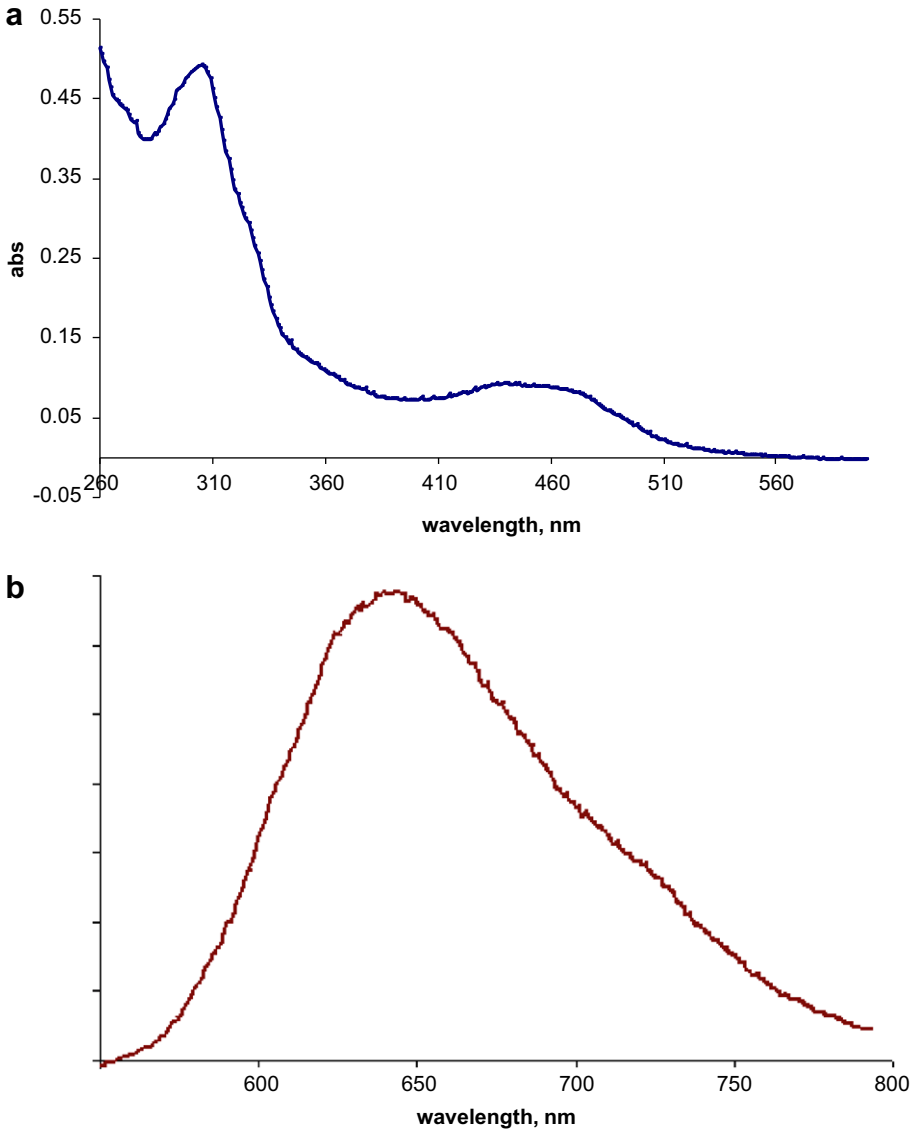

Fig. 4. (a) Absorption and (b) emission spectra of **9** in ethanol.

4.5.2. Emission spectra

The heavy metal atom (Ru) facilitates intersystem crossing via spin–orbit coupling, and the emission typically originates from the lowest lying triplet state (^{3}MLCT) [41]. The absorption and emission spectra of complex **9** in ethanol is shown in Fig. 4. The room temperature emission spectra of the complexes **5–16** (except compound **6**) showed red-shifted emission spectra, similar to those of other known Ru–MLCT complexes (Table 6). Compound **6**, containing only one PPh_3 ligand, did not have detectable emission at room temperature. It is significant that for this series of ligands that it is necessary to have two phosphine ligands in order to observe emission. This is most likely due to the more electron rich and more symmetrical structures of the bis-phosphine complexes, which could reduce distortion in the excited-state. The quantum yields (Φ) for the luminescent complexes in the presence of oxygen, listed in Table 6, were calculated relative to a Rhodamine B standard using Eq. (1). In general, these newly synthesized complexes showed higher quantum yields than $Ru(bpy)_3^{2+}$ (i.e. $\Phi > 0.06$).

Time-resolved luminescence decay measurements were performed by time-correlated single-photon counting (TCSPC). The data were analyzed by non-linear least-squares as described in the experimental section. The excited-state lifetimes of the luminescent complexes containing phenanthroline ligands (**5**, **11** and **13**) are in the range of 110–126 ns. However, complex **15**, which contains amino-phenanthroline ligand, has a lifetime of 250 ns. The bipyridyl complexes, when lacking the hydride ligand, have lifetimes of 180–200 ns. The hydride complexes **9** and **10**, at room temperature and in the presence of oxygen, had much longer lifetimes of 720 and 847 ns, respectively. The effect of oxygen on the photophysical properties of complexes **5**, **7**, **9**, **11** and **15** was also studied by measuring the lifetimes in both air-equilibrated and deoxygenated solutions in ethanol. The deoxygenated samples had longer excited-state lifetimes of 330, 680, 2630, 325 and 570 ns, for complexes **5**, **7**, **9**, **11** and **15,** respectively.

The anisotropy decay of complex **10** and **15** were studied in glycerol at 0 °C. The limiting anisotropy, which reflects the angle between the absorption and emission transition dipole moments, was 0.124 and 0.07, respectively, for complexes **10** and **15**. These values are higher than that (<0.01) observed for $Ru(bpy)_3^{2+}$ [5].

5. Conclusions

Several important conclusions can be drawn from these results. First, our original hypothesis that Ru(II) complexes with one diimine ligand and ancillary π-acceptor ligands will have longer excited-state lifetimes and higher quantum yields than previously reported for Os(II) complexes has been verified [24]. Furthermore, this series of complexes exhibit a wide range of excited-state lifetimes (110–850 ns), indicating that they will be useful for studying a wide range of dynamical biomacromolecular processes. The observed Stokes shifts and the emission wavelengths are similar to those obtained for Ru(II) complexes with two or three diimine ligands. The associated higher quantum yields relative to those previously reported for Ru(II) diimine complexes, also increases their usefulness. To help develop an understanding of the fundamental reasons for the observed variations in the photophysical properties we are now pursuing computational studies. Finally, the synthesis work reported here demonstrates the usefulness of the starting material **1** for making diverse ligand substitutions at the Ru(II) center. Although the low solubility of these complexes is an obstacle for using them in aqueous medium, their lipophilicity makes them promising for applications in lipid/membrane systems.

Acknowledgements

This research was supported by Grant CHE-0709738 from the National Science Foundation (NSF) [E.R.] and by Grants MCB-0517644 from NSF and RR15583 from the National Center for Research Resources (NCRR), a component of the National Institutes of Health (NIH) [J.B.A.R.].

Appendix A. Supplementary material

Supplementary data associated with this article can be found, in the online version, at doi:10.1016/j.jorganchem.2008.11.048.

References

[1] L. Li, H. Szmacinski, J.R. Lakowicz, Anal. Biochem. 244 (1997) 80.
[2] L. Li, H. Szmacinski, J.R. Lakowicz, Biospectroscopy 3 (1997) 155.
[3] L. Li, H. Szmacinski, J.R. Lakowicz, Anal. Biochem. 247 (1997) 465.
[4] L. Li, Chem. Phys. Lipids 99 (1999) 991.
[5] J.R. Lakowicz, Principles of Fluorescence Spectroscopy, 3rd ed., Springer, New York, 2006.
[6] G. Piszczek, Arch. Biochem. Biophys. 453 (2006) 54.
[7] J.V. Caspar, E.M. Kober, B.P. Sullivan, T.J. Meyer, J. Am. Chem. Soc. 104 (1982) 630.
[8] E.M. Kober, J.L. Marshall, W.J. Dressick, B. Sullivan, J.V. Caspar, T.J. Meyer, Chem. Phys. Lett. 91 (1982) 91.
[9] E.M. Kober, J.L. Marshall, W.J. Dressick, B.P. Sullivan, J.V. Caspar, T.J. Meyer, Inorg. Chem. 24 (1985) 755.
[10] C.V. Caspar, T.J. Meyer, J. Phys. Chem. 87 (1983) 952.
[11] C. Garino, S. Ghiani, R. Gobetto, C. Nervi, L. Salassa, V. Ancarani, P. Neyroz, L. Franklin, J.B.A. Ross, E. Seibert, Inorg. Chem. 44 (2005) 3875.
[12] E. Terpetschnig, H. Szmacinski, H. Malak, J.R. Lakowicz, Biophys. J. 68 (1995) 342.
[13] E. Terpetschnig, H. Szmacinski, J.R. Lakowicz, Anal. Biochem. 227 (1995) 140.
[14] H. Szmacinski, E. Terpetschnig, J.R. Lakowicz, Biophys. Chem. 62 (1996) 109.
[15] X.Q. Guo, F.N. Castellano, L. Li, J.R. Lakowicz, Anal. Chem. 70 (1998) 632.
[16] E.M. Kober, J.V. Caspar, B.P. Sullivan, T.J. Meyer, Inorg. Chem. 27 (1988) 4587.
[17] Felix N. Castellano, Xiang-Qun Guo, L. Li, Henryk Szmacinski, Jeffrey Sipior, Joseph R. Lakowicz, Proc. SPIE-Int. Soc. Opt. Eng. 3256 (1998) 223.
[18] B.P. Sullivan, J.V. Caspar, T.J. Meyer, Organometallics 3 (1984) 1241.
[19] T.A. Treadway, G.F. Strouse, R.R. Ruminski, T.J. Meyer, Inorg. Chem. 40 (2001) 4508.
[20] T. Tuyen, J.C.M. Nguyen, J. Am. Chem. Soc. 102 (1980) 7383.
[21] C. Garino, S. Ghiani, I. Bottero, R. Gobetto, C. Nervi, L. Salassa, E. Rosenberg, G. Caputo, G. Viscardi, I. Miletto, M. Milanesio, Eur. Inorg. Chem. 14 (2006) 2839.
[22] A. Albertino, C. Garino, S. Ghiani, R. Gobetto, C. Nervi, L. Salassa, E. Rosenberg, G. Viscardi, R. Buscaino, G. Croce, M. Milanesio, A. Sharmin, J. Organometal. Chem. 692 (2007) 1377.
[23] C. Garino, S. Ghiani, R. Gobetto, C. Nervi, L. Salassa, E. Rosenberg, J.B.A. Ross Xi Chu, K.I. Hardcastle, C. Sabatini, Inorg. Chem. 46 (2007) 8752.
[24] E.M. Kober, B.P. Sullivan, W.J. Dressick, J.V. Caspar, T.J. Meyer, J. Am. Chem. Soc. 102 (1980) 7383.
[25] SMART Version 5.628, Bruker AXS Inc., Analytical X-ray Systems, 5465 East Cheryl Parkway, Madison WI 53711-5373, 2003.
[26] SAINT Version 6.36A, Bruker AXS Inc., Analytical X-ray Systems, 5465 East Cheryl Parkway, Madison WI 53711-5373, 2002.
[27] SADABS Version 2.10, George Sheldrick, University of Göttingen, 2003.
[28] SHELXTL V6.12, Bruker AXS Inc., Analytical X-ray Systems, 5465 East Cheryl Parkway, Madison WI 53711-5373, 2002.
[29] A.A.J.C. Wilson (Ed.), International Tables for X-ray Crystallography, vol. C. Kynoch, Academic Publishers, Dordrecht, Tables 6.1.1.4 (pp. 500–502) and 4.2.6.8 (pp. 219–222), 1992.
[30] D. Collini, C. Femoni, M.C. Iapalucci, G. Longoni, P. Zanello, Special Publ. – R Soc. Chem. (Perspect. Organomet. Chem.) 287 (2003) 183.
[31] C.A. Parker, Photoluminescence of Solutions with Applications to Photochemistry and Analytical Chemistry, Elsevier, Amsterdam, 1968. p 262.
[32] M.D. Barkley, A.A. Kowalczyk, L. Brand, J. Chem. Phys. 75 (1981) 3581.
[33] R.E. Dale, L.A. Chen, L. Brand, J. Biol. Chem. 252 (1981) 7500.
[34] M.G. Badea, L. Brand, Methods Enzymol. 61 (1979) 378.
[35] J. Paoletti, J.B. Le Pecq, Anal. Biochem. 31 (1969) 33–41.
[36] B. Carlson, Inorg. Chim. Acta 357 (2004) 3967.
[37] G. Croce, M. Milanesio, D. Viterbo, C. Garino, R. Gobetto, C. Nervi, L. Salassa, CR Chim. 8 (2005) 1676.
[38] C. Garino, T. Ruiu, L. Salassa, A. Albertino, G. Volpi, C. Nervi, R. Gobetto, H.I. Hardcastle, Eur. J. Inorg. Chem. 23 (2008) 3587.
[39] H. Jacobsen, Helv. Chim. Acta 82 (1999) 297.
[40] S. Zalis, M. Krejcik, V. Drchal, A.A. Vlcek, Inorg. Chem. 34 (1995) 6008.
[41] T.J. Meyer, Pure Appl. Chem. 62 (1990) 1003.